AD-A128 951 COMPOSITE EQUATORIAL SPREAD-F WAVE NUMBER SPECTRA FROM 1/1
MEDIUM TO SHORT WAVELENGTHS(U) NAVAL RESEARCH LAB
WASHINGTON DC M SINGH ET AL. 01 JUN 83 NRL-MR-5088

UNCLASSIFIED F/G 20/9 NL

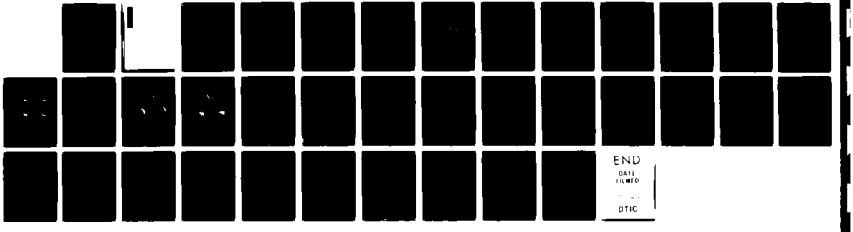

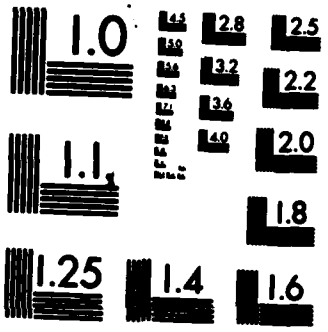

SECURITY CLASSIFICATION OF THIS PAGE (When Data Entered)

REPORT DOCUMENTATION PAGE		READ INSTRUCTIONS BEFORE COMPLETING FORM
1. REPORT NUMBER NRL Memorandum Report 5088	2. GOVT ACCESSION NO. AD-A128 957	3. RECIPIENT'S CATALOG NUMBER
4. TITLE (and Subtitle) COMPOSITE EQUATORIAL SPREAD-F WAVE NUMBER SPECTRA FROM MEDIUM TO SHORT WAVELENGTHS		5. TYPE OF REPORT & PERIOD COVERED Interim report on a continuing NRL problem. 6. PERFORMING ORG. REPORT NUMBER
7. AUTHOR(s) M. Singh* and E.P. Szuszczewicz		8. CONTRACT OR GRANT NUMBER(s)
9. PERFORMING ORGANIZATION NAME AND ADDRESS Naval Research Laboratory Washington, D.C. 20375		10. PROGRAM ELEMENT, PROJECT, TASK AREA & WORK UNIT NUMBERS 61153N; RR033-02-44; 41-0949-0-3
11. CONTROLLING OFFICE NAME AND ADDRESS Office of Naval Research Arlington, VA 22217		12. REPORT DATE June 1, 1983 13. NUMBER OF PAGES 35
14. MONITORING AGENCY NAME & ADDRESS(if different from Controlling Office)		15. SECURITY CLASS. (of this report) UNCLASSIFIED 15a. DECLASSIFICATION/DOWNGRADING SCHEDULE

16. DISTRIBUTION STATEMENT (of this Report)

Approved for public release; distribution unlimited.

17. DISTRIBUTION STATEMENT (of the abstract entered in Block 20, if different from Report)

18. SUPPLEMENTARY NOTES

*Present address: Sachs/Freeman Associates, Inc., Bowie, MD 20715

19. KEY WORDS (Continue on reverse side if necessary and identify by block number)

Equatorial Spread-F	Transitional wavelengths	Lower-hybrid instability
Ionospheric irregularities	Meter-size irregularities	
Wave number spectra	Rayleigh-Taylor instability	
Intermediate wavelengths	Gradient-drift instability	

The authors

20. ABSTRACT (Continue on reverse side if necessary and identify by block number)

In an effort to provide a full-spectral classification of equatorial spread-F irregularities from large scale behavior (~100 km) to the meter-size domain, we have analyzed a combination of rocket and satellite data which in concert covers the complete six decade irregularity distribution. Our results provide a composite perspective in the hierarchy of processes which contribute to the total phenomenon called equatorial spread-F and

Their

(Continues)

DD FORM 1 JAN 73 1473 EDITION OF 1 NOV 65 IS OBSOLETE
S/N 0102-014-6601

SECURITY CLASSIFICATION OF THIS PAGE (When Data Entered)

20. ABSTRACT (Continued)

provides the first "in situ" meter-size irregularity measurements which help explain the relationship of spectral power at short wavelengths to that in the transitional and intermediate domain. In a synoptic perspective we find that the medium and intermediate wavelength domain display $k^{-1.5}$ and $k^{-2.5}$ behaviors respectively, in both vertical and horizontal distributions. The transitional wavelengths ($\lesssim$ 200 m $\rightarrow$ 20 m) are dominated by a steep $k^{-4.7\pm0.3}$ universal-drift-wave spectral behavior but breaks at $kr_i \gtrsim 1$ ($\lambda \lesssim$ 20 m) to much higher power levels...a result which is consistent with ground based radar results in the meter-scale domain. Our shortest wavelength results (1 m $\lesssim \lambda \lesssim$ 20 m) are qualitatively consistent with a lower-hybrid-drift wave interpretation but the presence of resonant structure in the observed spectral distribution strongly suggest a resonant wave-particle-interaction process.

CONTENTS

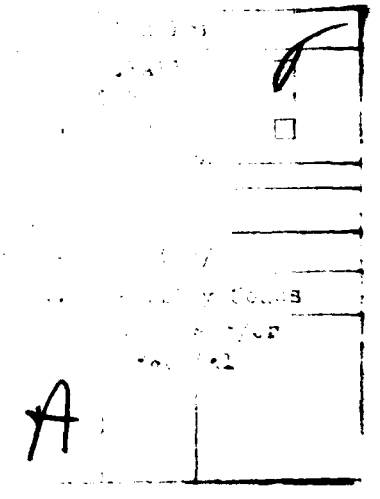

COMPOSITE EQUATORIAL SPREAD-F WAVE NUMBER SPECTRA FROM MEDIUM TO SHORT WAVELENGTHS

INTRODUCTION

Equatorial spread-F has been the subject of intensive investigation, with advances in observational capabilities and computational modelling having contributed in a synergistic way to a much improved understanding of the phenomena (Matsushita, et al., 1981a,b). Historically, analysis of spread-F irregularities had its beginning in linear theories with Dungey (1956) the first to suggest that equatorial spread-F was initiated on the bottomside F-layer gradient by the Rayleigh-Taylor instability. Driven by the meter-size irregularity distributions observed by ground-based radars (Woodman and LaHoz, 1976) and the concurrent large scale plasma holes measured "in situ" (McClure et al., 1977; Basu et al., 1978; Szuszczewicz 1978), theoretical efforts focussed on establishing various descriptions of spectral distributions over the broad range of structures identified with the phenomena (Figure 1). Initially it was thought that planetary scale irregularities (due to aeronomic effects and tidal waves) could cascade to km-size dimensions, trigger the Rayleigh-Taylor process and through a power law dependence distribute the energy down to the meter range. However, a pure cascade of energy from long to short wavelengths could not explain the observational results when Woodman and Basu (1978) extrapolated the spectral behavior of "in situ" medium-to-intermediate scale irregularities ($\gtrsim$100 meters to 10 km) down to the Jicamarca measurement size at 3 meters. It was generally accepted that a $k^{-2.0}$ to $k^{-2.5}$ behavior ($k \equiv 2\pi/\lambda$) represented

Manuscript approved March 10, 1983.

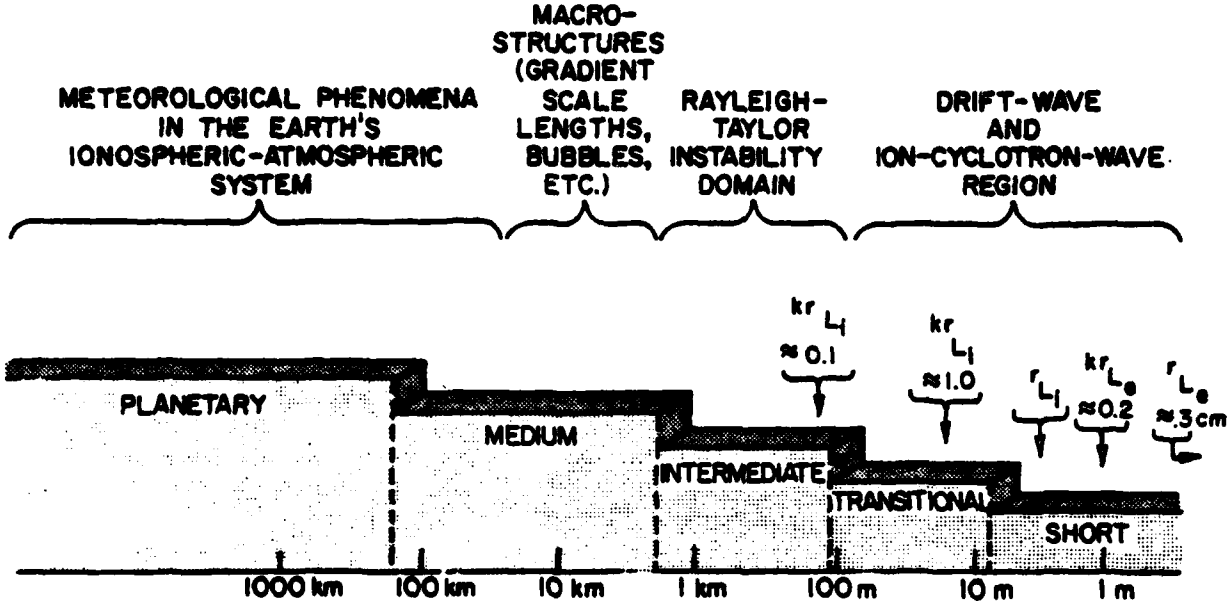

Fig. 1 — A simplified synoptic perspective of the full domain of equatorial F-region irregularities with contributing mechanisms. Characteristic lengths are the wave number $k=2\pi/\lambda$, and the ion and electron gyroradii, r_i and r_e, for $M_i = 16$, $T_e = 1350\ ^\circ K$, $T_i \sim 500\ ^\circ K$ and $B = 0.3$ gauss.

the spectral distribution for medium-to-intermediate scale irregularities but the extrapolation to the 3 meter regime suggested the presence of significantly more power than that supported by the radar measurements. An exponential-like cut-off near the ion gyroradius (r_i) was proposed to explain the disparity but that too had problems in explaining the results of Tsunoda et al. (1979) and Towle (1980) who reported Altair radar results inconsistent with an exponential fall-off assumption. Kelley et al. (1982a) suggested that the $k^{-2.0}$ to $k^{-2.5}$ spectrum did not break exponentially but rather to a steeper power law dependence ($\propto k^{-4.5}$) determined by drift waves. This proposal appeared to support the observations in the transitional wavelength regime ($\propto$20-200 meters) but was still inconsistent with the meter and sub-meter Altair observations. Retrofitting a number of ideas suggested that in the shortest wavelength regime (1 m $\lesssim \lambda \lesssim$ 20 m) the spectrum had to be shallower than $k^{-4.5}$ and that there was some other scale near $kr_e \propto 1$ (r_e = electron gyroradius) below which the spectral distribution had another variation as discussed by Huba and Ossakow (1979, 1981a,b). According to Kelley et al.(1982b) the resolution of spectral behavior in this transition to short wavelength regime remained as one of the outstanding problems in a complete understanding of equatorial spread-F phenomena.

To provide a full spectral classificiation of spread-F irregularities from large scale behavior ($\propto$ 100 km) to the heretofore undetermined meter-size domain we have analyzed a combination of rocket and satellite data which in concert covers

the full spectral regime. Our results provide a composite perspective in the hierarchy of equatorial spread-F processes and provides the first "in situ" meter size measurements which help explain the small scale size irregularity distributions that have given rise to intense backscatter returns in ground-based radar observations.

IRREGULARITY DISTRIBUTIONS

a. Vertical Wave Number Results

The vertical wave number data reported in this paper were provided by a pair of pulsed plasma probes aboard the Plumex-I rocket (Szuszczewicz et al., 1980). The rocket payload, with a full thermal plasma diagnostics complement (pulsed plasma probes, mass spectrometer, electric field sensors, and two-frequency beacon), was launched into well-developed equatorial spread-F. The experiment incorporated coincident east-west Altair radar scans in a plane that included the penetration of the rocket's upleg trajectory. The right-hand panel of Figure 2 shows the upleg measurements of relative electron density as represented by electron-saturation ($I_e(V^+)$) current. Evident in the profile are a large number of electron density depletions which are distributed from the bottomside (region C) to the topside F-layer (region H through K). The largest depletion is in the region H-I where the change in electron density was found to be about 80%. The left-hand inset in Figure 2 presents the Altair radar map with the superposition of the Plumex rocket trajectory (from about 200 to 248 sec in the upleg trajectory) crossing the depletion G, H and I. The radar map shows that maximum radar

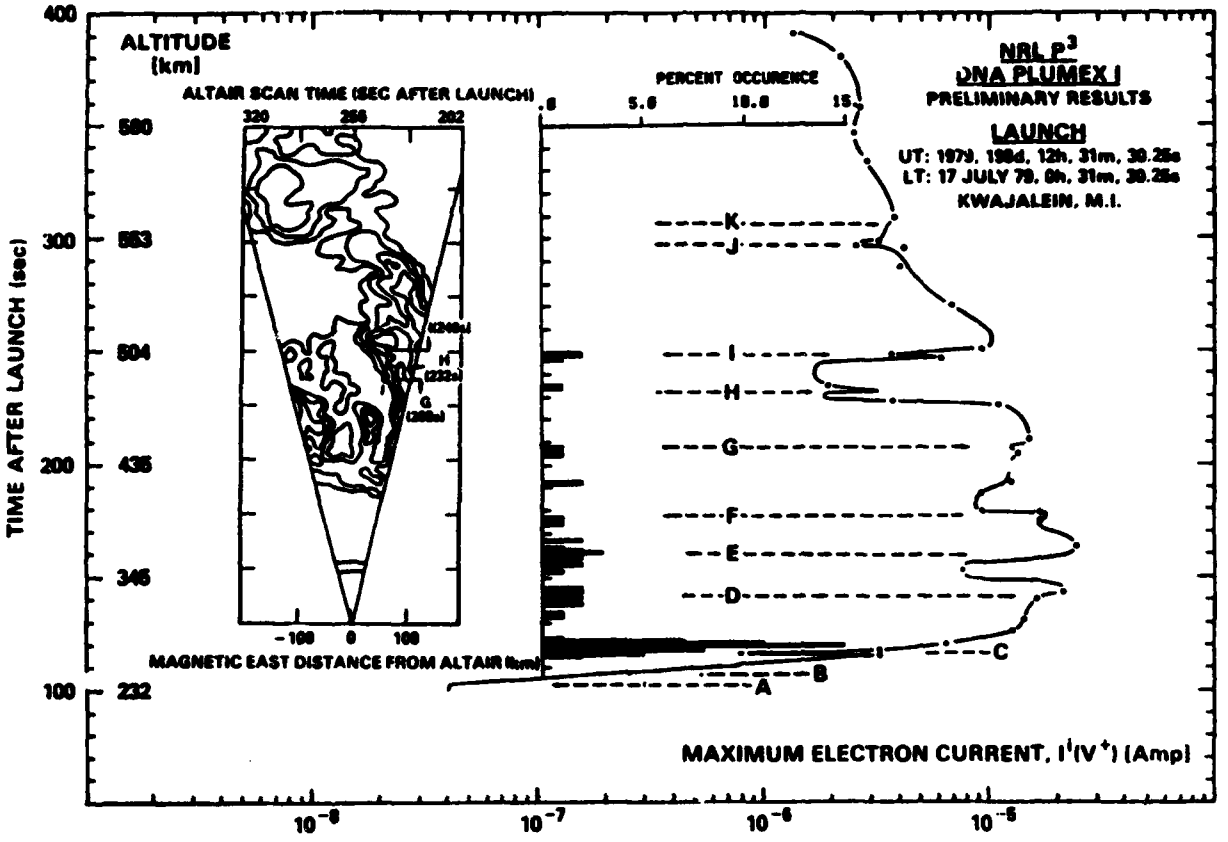

Fig. 2 — Equatorial F-region profile under spread-F conditions. Left-hand inset is Altair 0.96 meter backscatter plot showing superposition of a segment of the rocket trajectory corresponding to the actual "in situ" density profile displayed on the right. $I^{i}\ (v^{+}) \propto N_e$. The center panel is a histogram presentation of gradient scale lengths $\leq$ 200m. (Figure adapted from Szuszczewicz, et al., Geophys. Res. Lett. 7, 537, 1980.)

returns (from 0.96 m irregularities) originated on the topside wall of the H-I depletion (Szuszczewicz, et al., 1980).

Szuszczewicz and Holmes (1980) have performed the power spectral analyses of irregularities within the bottomside depletion "C", and the results yielded a one-dimensional spectral index between 2.0 and 2.5 (n in equation $P_{Ne} \propto k^{-n}$), primarily in the intermediate wavelength domain. Focussing on region C, with gradient scale lengths between 8 and 25 km, Keskinen et al. (1981) performed analytical nonlinear studies and numerical simulations based on the collisional Rayleigh-Taylor instability taking into account F-layer conditions of vertical drift velocity and gradient scale lengths. The analytical and computational results showed that large depletions and associated smaller scale structures can develop on time scales of several thousand seconds and yield a one-dimensional spectral index 2.5. This agreement with the observed power spectra supported the contention that the collisional Rayleigh-Taylor instability was responsible for the intermediate wavelength irregularity distribution on the unstable bottomside gradient under conditions of equatorial spread-F.

Kelley et al. (1982a), using a fixed-bias electrode on an electric field boom, analyzed substantially larger portions of the F-region shown in the Figure, and attempted to generate a unified model for spread-F irregularities. They discussed aeronomic effects and atmospheric dynamics at the largest scales, a generalized Rayleigh-Taylor instability at intermediate scales, and a cascade process involving drift waves at transitional wavelengths. Limited to a capability of detecting plasma

structures with $\lambda \gtrsim 20$ m they were unable to study the short wavelength domain and found extrapolations of their transitional wavelength results to the meter regime inconsistent with the Altair results in regions of largest radar returns. Using the more sensitive technique of the pulsed-plasma-probe we now conduct an expanded analysis of the transitional wavelength behavior and investigate the spectral features in the short wavelength domain down to dimensions approaching $\lambda = 1$ m.

The pair of pulsed plasma probes aboard the Plumex-I had a sampling rate of 2048 Hz each. There were two modes of operation applied to the probes, baseline and pulsed sweep (Holmes and Szuszczewicz, 1975 and 1981). In the baseline mode, all samples yielded electron (ion) saturation currents (proportional in first order to electron (ion) density) with a Nyquist frequency for FFT analyses at 1024 Hz. This capability corresponded to a 2 meter resolution for the bottomside depletion (c) and 1 meter for the topside (H-I region) depletions. In the pulsed sweep mode, a pulse-modulated sweep was applied to the probe, alternating sampling between baseline and sweep currents (for determination of electron density and temperature). The two modes were applied alternately to each of two probes for 10 second periods maintaining a minimum 1024 Hz Nyquist frequency at all times throughout flight.

For purposes of discussing the transitional wavelength domain, Figure 3 shows four power spectra (using a Hanning window and a low frequency filter below 3 Hz), selected at different altitudes extending throughout the F-layer. Figure 3a presents

results at an altitude of 286.1 km (121 secs after liftoff) on the topside wall of depletion C. The power spectral index in the approximate spatial wavelength domain of 20-200 m is shown to be 4.7. The power spectra in Figure 3b through 3d are associated with depletions D, E and G respectively, with power spectral indices between 4.8-5.0 in the transitional wavelength domain. Similar power spectra have been found at a number of places along the up- and downleg trajectories at altitudes above about 282 km.

Transitional wavelength power spectra with the indices between 4.5-5.0 are considered to be produced by a universal drift instability (Kelley et al., 1982a; Gary et al., 1983) driven by gradient scale lengths less than a few hundred meters. To investigate possible correlations between steep gradients and spectra like those in Figure 3, we have calculated the gradient scale lengths $L = N_e(dN_e/dX)^{-1}$ with $dX \equiv \Delta X = 100$ m (sliding each calculation-domain 50 m along the entire trajectory). The results for gradient scale lengths less than 200 m are produced as a histogram in the central panel of Figure 2. This histogram shows the relative percent occurrence of gradient scale lengths less than 200 m from 110 sec to 270 sec in time after-lift-off, covering all the depletions on the upleg trajectory. Evident is the observation that small gradient scale lengths occur at a large number of places in the F-layer. More importantly however, we note that all these locations of small gradient scale lengths were populated with transitional and/or short wavelength spectra of substantial power levels above the system noise.

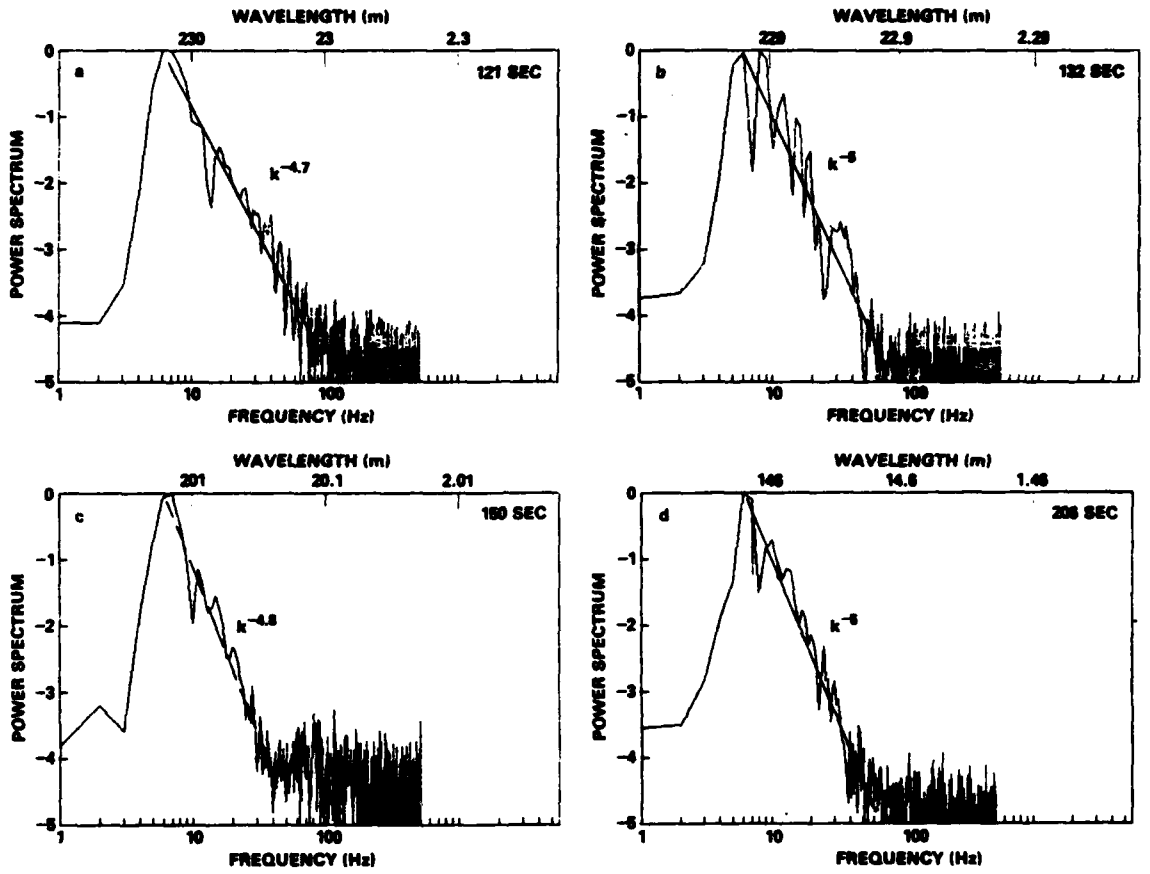

Fig. 3 — Sample of transitional wavelength power spectra. Measurements are made in the frequency domain and wavelength definitions result from a vehicle velocity/frequency transformation.

In our search for defineable spectral behavior in the short wavelength domain ($\lambda \lesssim 25$ m) we found that the FFT results tended to suffer from the steep $k^{-4.7\pm0.3}$ behavior in the intermediate domain, in most cases rendering power at the shorter wavelengths below the noise level (e.g., Figure 3). However, just above the topside H-I depletion we found substantive short wavelength results. This is significant since this is the region along the rocket trajectory in which Altair radar measured maximum returns from 0.96 meter irregularities. Figure 4 presents the associated "in situ" spectral behavior with two features of particular note: first, in the top panel there is a marked change in spectral behavior near $k\ r_i=1$ (where r_i is the ambient ion gyroradius); and second, there is another break in the wavelength (frequency) dependence near $k\ r_e = 0.06$. (The point $k\ re = 0.06$ also corresponds to $kr_i \lesssim 10$). The same features can be identified in the two lower panels, but with diminished prominence. The power of these short wavelengths is substantially above the noise and thought to be generated by the lower hybrid drift instability that has been argued to exist in the regime $k\ r_e \lesssim 1$ (Huba and Ossakow, 1981a).

Measureable short wavelength power was also observed in $L \leq 200$ m domains other than in the topside of the H-I depletion; however the spectral characteristics were considerably different from those displayed in Figure 4. Notable features of the other short wavelength observations are presented in Figure 5 where the spectra show peaks in frequency ranging from 170 Hz to 480 Hz with corresponding spatial wavelengths lying between 10 and 3.5

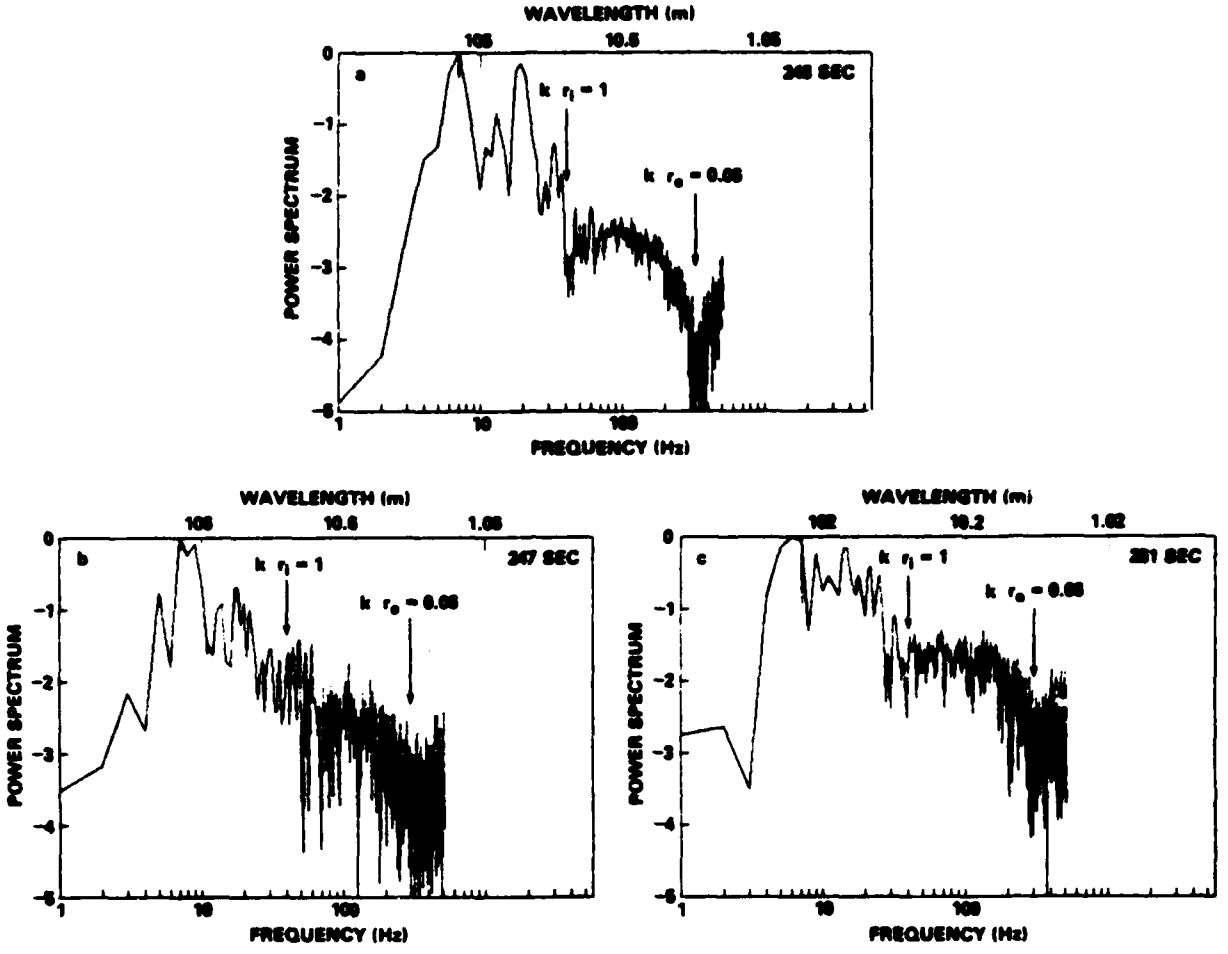

Fig. 4 — Short wavelength spectral distributions in the topside region of the H-I depletion (Figure 2). r_e and r_i are the electron and ion gyroradii respectively. The spectra show a marked departure from the transitional $k^{-4.7\ (\pm.3)}$ behavior (Figure 3) with a "softening" of the distribution (the lower left panel fits a $k^{-1.5}$ distribution) and/or a non-uniform behavior with transitions near $kr_i = 1$ and $kr_e = 0.06$, the latter point corresponding approximately to $\lambda = r_i$.

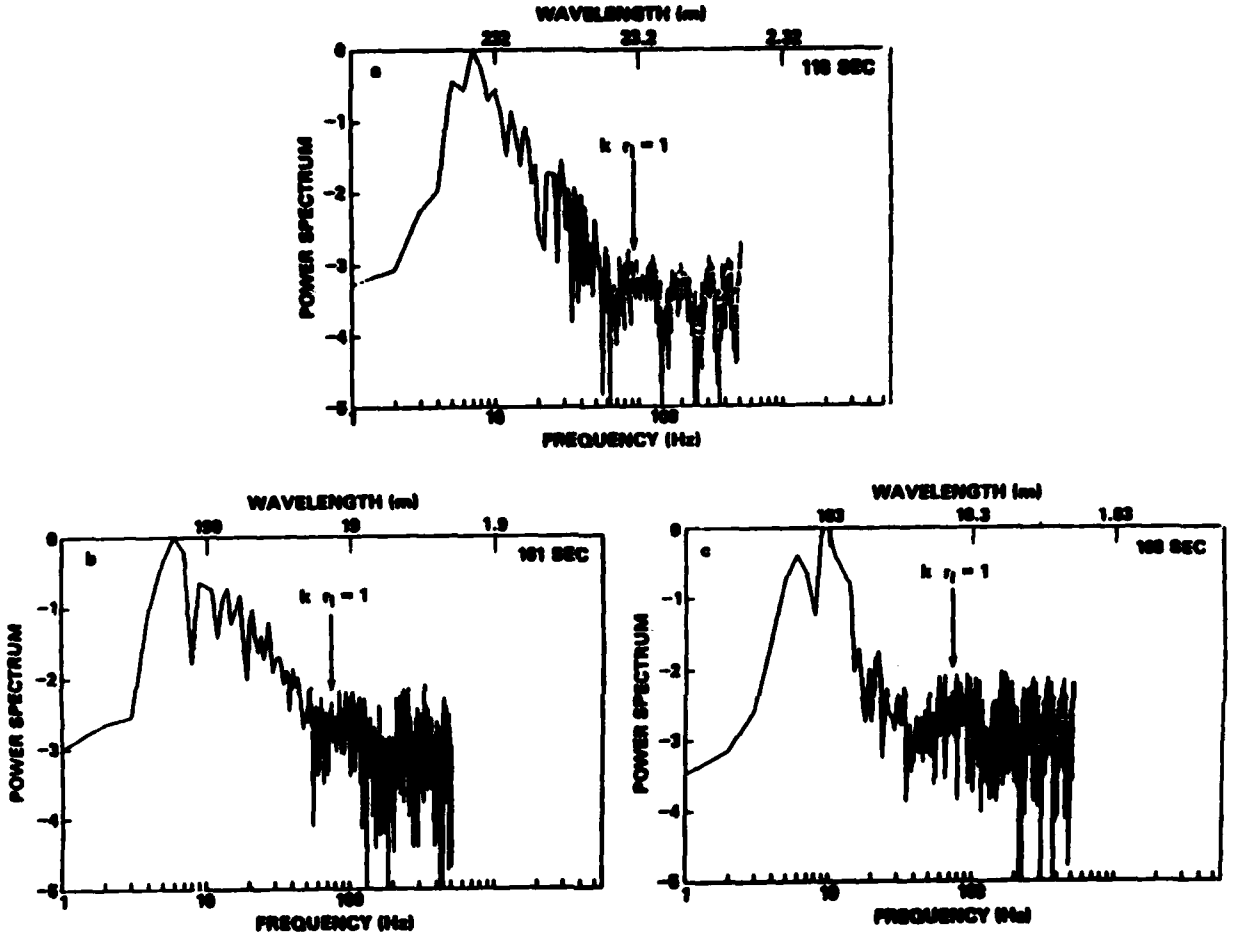

Fig. 5 — Transitional-to-short wavelength spectra showing major differences in the two domains.

meters, respectively. The equal power levels for the multiple peaks in each of the spectra suggest that they are not harmonics of a single frequency. To identify possible causal mechanisms we present in Figure 6 collisionless linear theory dispersion relations for a number of low frequency modes with $\beta = 8\pi N_e kT_e/B^2 << 1$, $v_a[\equiv B(4\pi N_e M_i)^{-1/2}] >> v_s[\equiv (kT_e/M_i)^{1/2}]$ and $\omega_D/2\pi = kT_e/L_e B\lambda N_e$. β, v_a, v_s and $\omega_D/2\pi$ are the thermal-to-magnetic energy ratio, the Alfven velocity, the ion sound speed, and electron drift frequency, respectvely. The curves have been drawn using observed values for electron temperature ($T_e = 1350^o$ K), ion mass (m_i=16) and gradient scale lengths (L=200m). For parametric ranges encompassing the actual observations ($\lambda \gtrsim 20$ meter, $50 \lesssim F$ [Hz] $\lesssim 500$), the results in Figure 6 point to the ion-cyclotron, ion-acoustic and drift-wave modes as the obvious candidates contributing to the observed spectral features at short wavelengths. At any given wavelength, the simple linear theory predicts the existence of three frequencies, and allowing all short wavelengths to exist, suggests the possibility of a broadband spectral distribution rather than a power law k^{-m} dependence as suggested by Tsunoda (1980). Our short wavelength data supports a resonance-like mode-coupling and/or modified-broadband spectral distribution as opposed to a simple power law. More importantly however is the experimental confirmation of what has been suspected for some time...that the steep power law dependence ($\gtrsim k^{-4.5}$) in the intermediate wavelength domain cannot be extrapolated to shorter wavelength since "predicted" power levels are too low to be

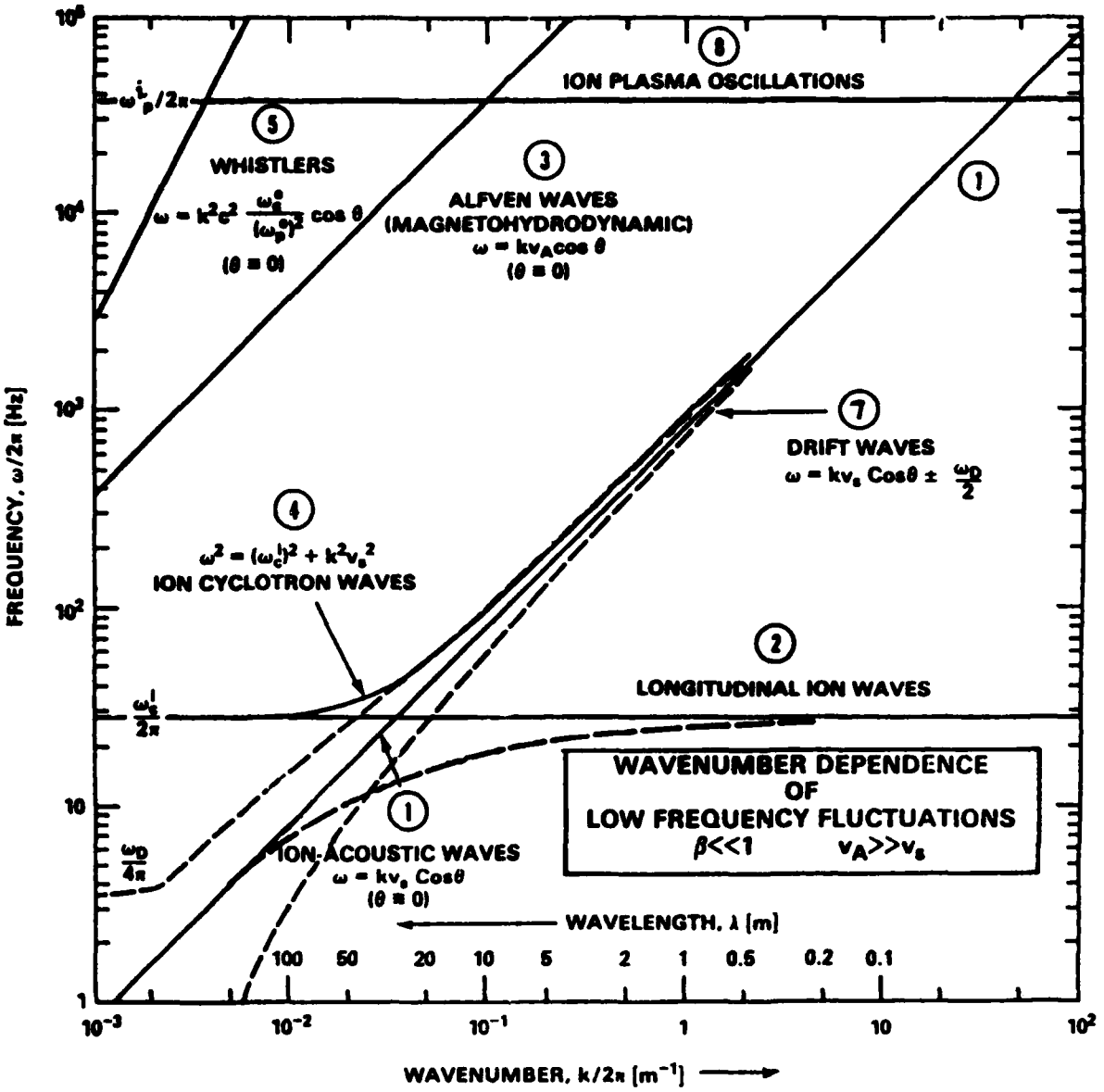

Fig. 6 — Linear theory dispersion relations for collisionless transitional-to-short wavelength modes in a magnetoplasma. The following parametric values have been assumed: $n_e = n_i = 10^6$ cm^{-3}, $T_e = 1350$ °K, $m_i = 16$ amu, $B = 0.3$ gauss.

consistent with the meter-like results of Jicamarca and Altair radars. Indeed, the short wavelength regime manifests a marked departure from the spectral behavior in the transitional region...that marked departure occurring at a spatial domain nominally observed $kr_i \gtrsim 1$ where r_i is the 0^+ gyroradius (2.8 meter at B = 0.3 gauss). Additional discussion of the short wavelength phenomena will be advanced in subsequent sections.

b. Composite Vertical Spectral Distributions

A composite representation of the density irregularities observed in the Plumex vertical profile data is presented in Figure 7 for wavelengths extending from 20 km to 2 m. We have made the following observations:

1. The medium wavelength region ($\gtrsim$ 1 → 20 km) has a relatively soft spectral index at 1.5. Although no power spectra covering this domain have been shown in the present paper, analyses have been conducted throughout the trajectory and found to be consistent with other published results in this wavelength domain (Livingston et al., 1981). This spectral behavior has been described by Kelley and Ott (1978) as a simple two-fluid process in which a rising low density F-region bubble generates a wake consisting of vortices in the background plasma with initial scale sizes comparable to the bubble dimensions. According to Kelley and Ott (1978) the subsequent interaction with background density gradients results in a turbulent cascade with a k^{-1} spectral behavior. The k^{-1} spectral prediction is softer than that found in accumulating data sets (e.g., $k^{-2.0}$ in Dyson et al.,1974; Kelley et al., 1976; and Morse et al., 1977),

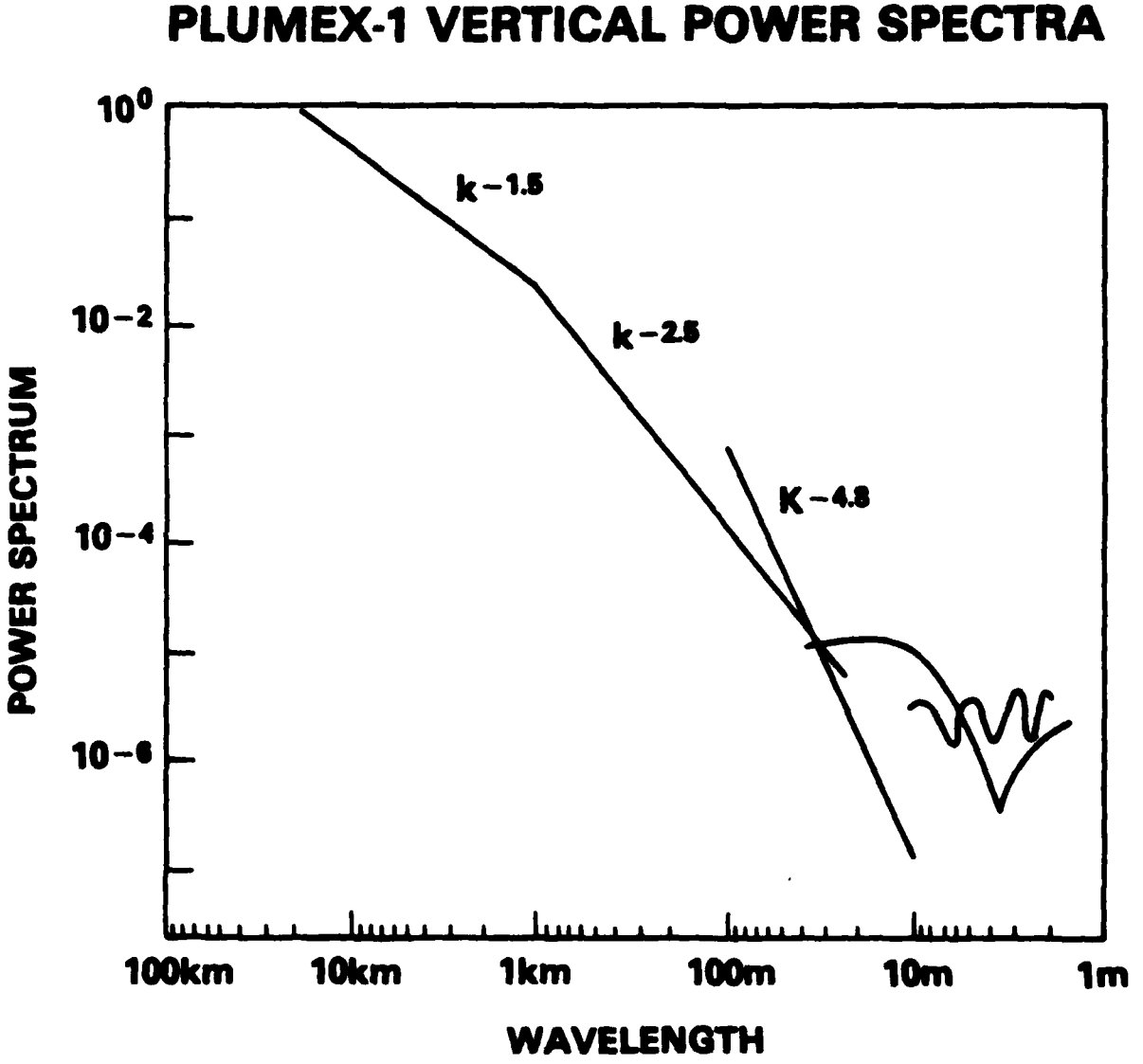

Fig. 7 — Synthesized vertical power spectral distributions covering the medium, intermediate, transitional, and short wavelength domains.

but not inconsistent with a $k^{-1.5}$ observation which can reflect the influence of a $k^{-2.0}$ behavior introduced at edges of macroscale structures.

2. The intermediate wavelength domain ($\gtrsim$ 0.05 → 2 km) manifests spectral indices between 2 and 2.5 as shown by Szuszczewicz and Holmes (1980), with similar results having been reported from complementary measurements (Rino et al., 1981, Szuszczewicz et al., 1981, and Singh et al., 1982). In addition, analytical studies and numerical simulations based on the collisional Rayleigh-Taylor instability have yielded two-dimensional vertical and horizontal "in situ" power spectral indices between 2 and 2.5, supporting the belief that intermediate wavelength irregularities are produced by the collisional Rayleigh-Taylor instability (Keskinen et al., 1981).

3. The transitional wavelength domain (20-200 m) shows steep spectra with indices between 4.5 and 5.0. Moreover, such spectra tend to be co-located with steep density gradients (e.g., gradient scale lengths less than 200 m). Similar observations have also been reported by Kelley et al., (1982a). A suggested mechanism for the generation of these irregularities is the universal drift instability, known to excite drift waves at $kr_i \leq 1$ with spectral indices in the range 4.5 to 6 (Costa and Kelley, 1978; Kelley et al., 1982a).

4. In the short wavelength domain ($\lambda \lesssim$ 20 m) two types of phenomena are observed: First, there are spectra which show marked breaks near 3 m wavelength (see Figure 4) in a specific ionospheric domain where Altair radar shows maximum returns from

0.96 m irregularities. This break corresponds to (kr_e, kr_i) ≈ (0.06, 10) and we note the suggestion that very small scale irregularities can be generated by the lower hybrid instability in the regime $kr_e \lesssim 1$ (Huba and Ossakow, 1979, 1981a, b) There is another break at the longer wavelength end of the short wavelength spectra...that break occurring at $kr_i \gtrsim 1$ where universal drift waves are expected to transition from an unstable to a stable configuration. The second type of short wavelength observation (See Figure 5) shows spectral peaks corresponding to meters in wavelength and a few hundred Hz in frequency which are likely to be the result of drift waves, ion cyclotron waves or mode-coupling as discussed in the preceding section.

C. Horizontal Wave Number Spectra

The data presented thus far has dealt only with the vertical distribution of irregularities in a single rocket investigation. While the spectral index in each of the different wavelength domains is a manifestation of the active geoplasma processes, care should be exercised in any attempt to uniquely identify any spectral index with a specific mechanism. Irregularity distributions are clearly a function of time in the overall process and can be modified by changing ionospheric conditions as well as transport and diffusion. With this thought we have supplemented the rocket data with an analysis of S3-4 satellite data (Szuszczewicz, et al., 1982a,b). With this additional information we can develop a perspective on the horizontal spectral distribution and perform a statistical sampling of spectral behavior in specific wavelength domains.

The data for our study of spread-F irregularities in the horizontal direction was made available by a pair of pulsed-plasma-probes (P^3) aboard the STP/S3-4 satellite (Szuszczewicz, et al., 1982a), orbiting at lower F-region altitudes with sun synchronous nighttime equatorial crossings near 2230 LT. One of the probes was biased to respond to the variations in plasma electron saturation currents ($I_e \propto N_e$) and the other probe responded to ion saturation currents ($I_i \propto N_e / \sqrt{m_i}$). Subject to the selection of a number of commandable modes of operation, either probe could be repetitively pulsed from its fixed-bias level to generate conventional Langmuir characteristics for full determination of electron density N_e, electron temperature T_e and the plasma potential V_p (Holmes and Szuszczewicz, 1975, 1981). Scale lengths as small as 20 meters were sampled in a high data format. The modes of operation and the experimental details are discussed by Szuszczewicz et al., (1982a).

The middle panel in Figure 8 shows a sample of "in situ" S3-4 electron density measurements during a nighttime equatorial crossing. The in-track profile shows a number of depletions with the depletion level ranging from factors of $\sim$ 3 to $\sim$ 100. The middle panel shows the density averaged over one data cycle (1 data cycle = 0.96 sec or 7.2 km), while the top panel shows the maximum relative fluctuations ($\Delta N_e/N_e$) about the averaged value. The bottom panel shows the corresponding values for $(\Delta N_e)_{rms}$.

To study the spectral behavior in the horizontal direction, we have divided the wavelength regions into three domains: medium scale (1 to $\sim$ 60 km), intermediate (80 m to 2 km), and

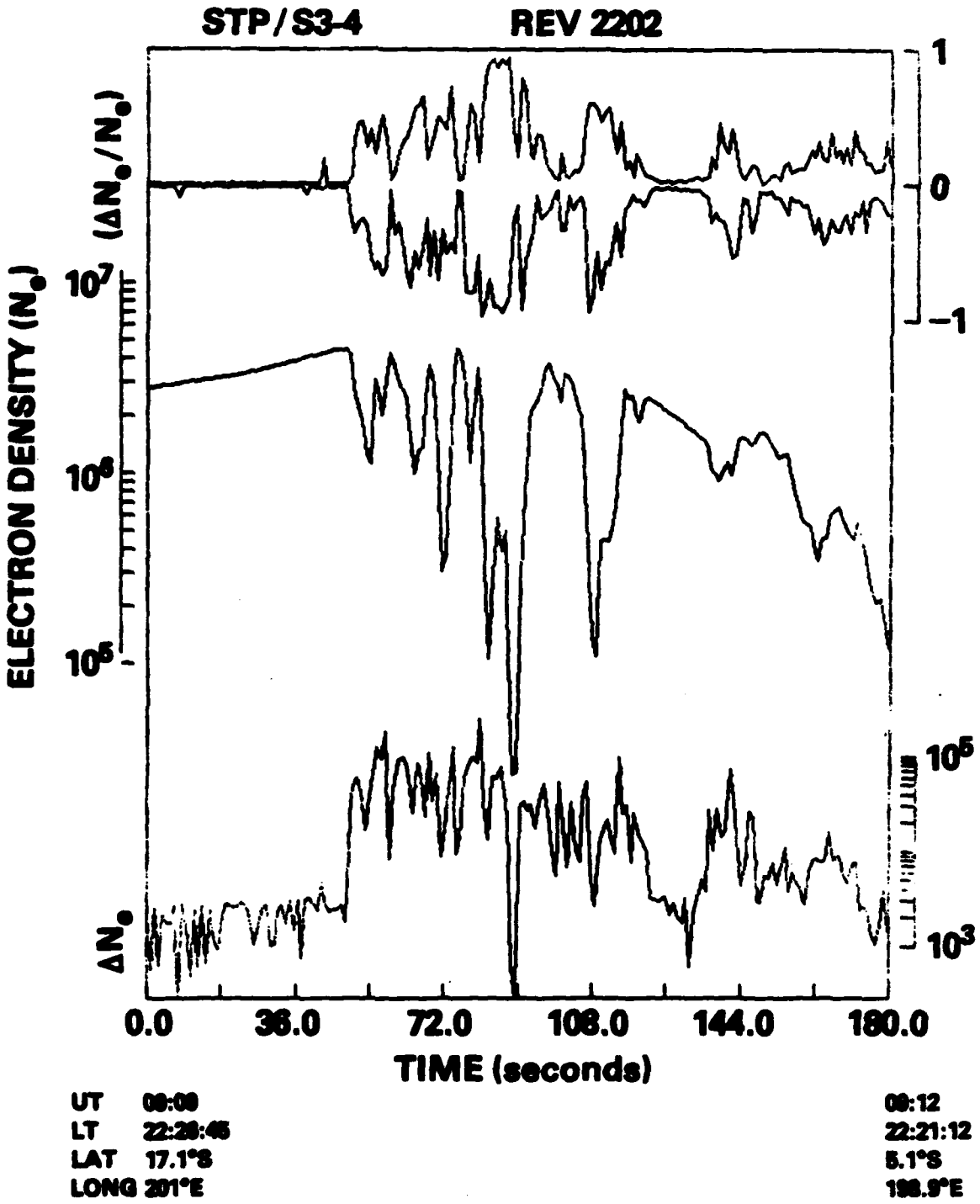

Fig. 8 — "In situ" equatorial irregularity S3-4 data collected during rev 2202.

transitional ($\lambda < 200$ m). The synoptic results, which we are about to present, are based on the spectral analyses of four equatorial crossings during the occurrence of spread-F (revs 2202, 2186, 2122 and 2123). All were recorded in the fast-rate mode with sampling at 800 Hz (Nyquist frequency = 400 Hz). For analyses of the medium wavelength regime, the data were decimated by a factor of 12. The results of nearly 300 spectra were routinely analyzed, and the spectral power dependence was computer fitted in the different wavelength regimes to determine the associated spectral index. The results were compiled in a statistical format and the frequency of occurrence of individual indices plotted in Figure 9 as a histogram for each wavelength domain. The upper panel shows that the spectral index in the medium wavelength domain peaks near 1.5, with a scatter in the index from 0.8 to 2.0. The most probable and average values for the spectral index in this region was found to be 1.4 with a standard deviation of 0.06. In the intermediate wavelength domain the power spectral index peaked near 2.45, with values ranging from 1.6 to almost 3.8. The most probable and median values are 2.4 and 2.5 respectively with the standard deviation of 0.22. In the domain of transitional wavelengths (i.e., $\lambda < 200$ m), the histogram shows that the spectral index can lie between 0 and 3 without a strong indication of a most probable value.

The results in Figure 9 can also be presented in power spectral format (see Figure 10) to facilitate comparison with the vertical-format rocket-borne analyses (Figure 7). Vertical and horizontal irregularity distributions in the medium and

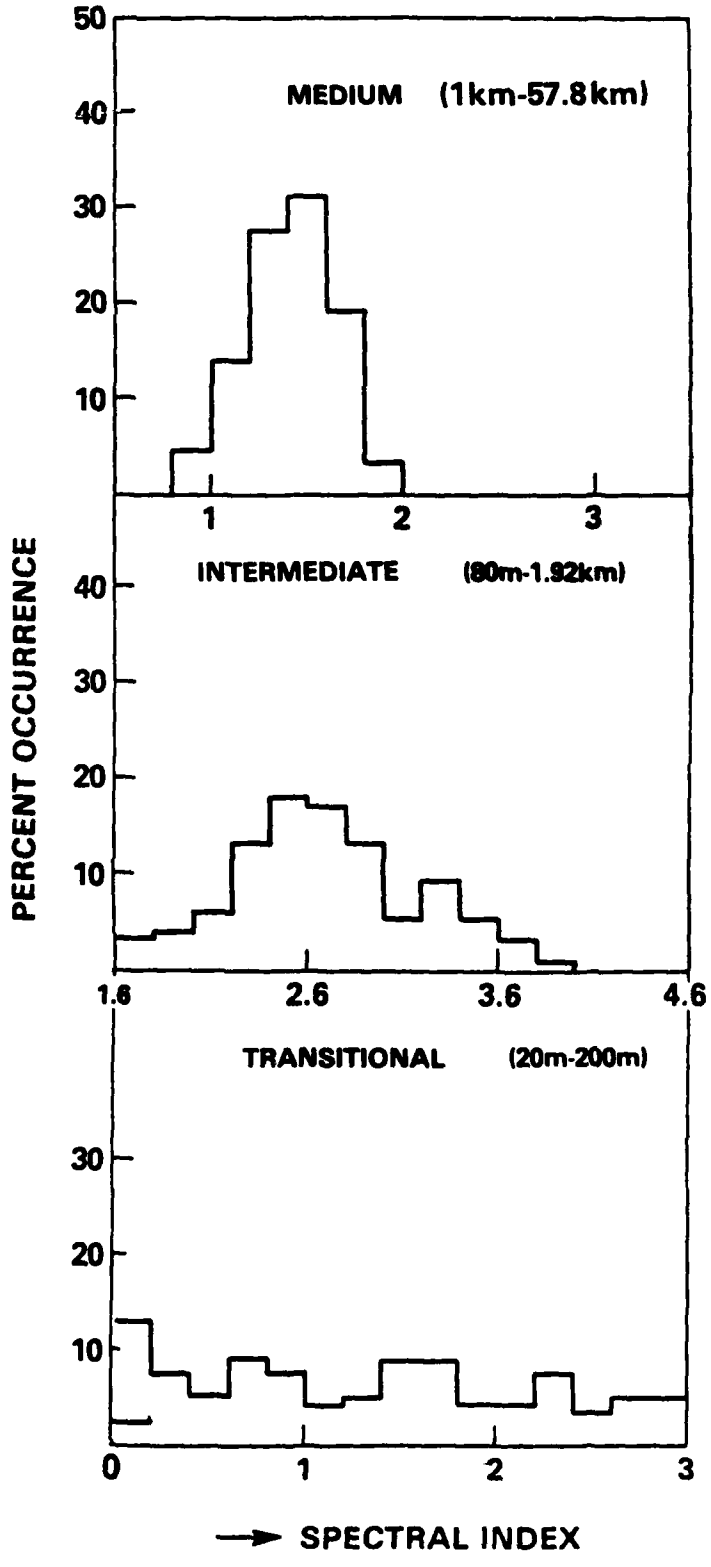

Fig. 9 — Histogram presentation of horizontal wavelength spectral indices covering the medium, intermediate and transitional domains.

intermediate wavelength regimes are seen to be virtually identical (Compare Figures 7 and 10). A major difference exists in the transitional regime ($\lambda < 200$ meters) where the steep $k^{-4.7}$ behavior in vertical structure has no counterpart in horizontal distributions. We believe that this is a simple manifestation of collisional damping of the drift wave modes at lower altitudes (Gary et al., 1983) since the S3-4 data were accumulated at altitudes $\lesssim$ 270 km. In the horizontal domain, we interpret the $k^{-1.3(0.86)}$ behavior as a simple averaging of extended intermediate wavelength behavior ($k^{-2.5}$) with cases in which the $\lambda \lesssim$ 200 m results were in the system noise. No physical process should be identified with the $k^{-1.3}$ distribution at transitional wavelengths.

The results in Figure 10 can also be compared with the measurements made on OGO-6 (Dyson et al., 1974) and on AE-E (Livingston, et al., 1981). The OGO-6 results showed a power spectral index near 2 for the 70 m to 7 km domain and the AE-E observations showed a spectral index near 2 in the km-to-hundreds of kilometer region. If analyzed over the same dimensions, the S3-4 results would tend to average the medium and intermediate behavior resulting in a spectral behavior steeper than 1.5 but softer than 2.5, that is, approaching 2.0.

COMMENTS AND CONCLUSIONS

Equatorial spread-F irregularities covering nearly a 6-decade wavelength domain have been experimentally "catalogued" and explained by invoking a hierarchy of mechanisms. The data sources have been the PLUMEX rocket campaign and the S3-4

S3-4 HORIZONTAL BOTTOMSIDE F-REGION (ESF) POWER SPECTRA

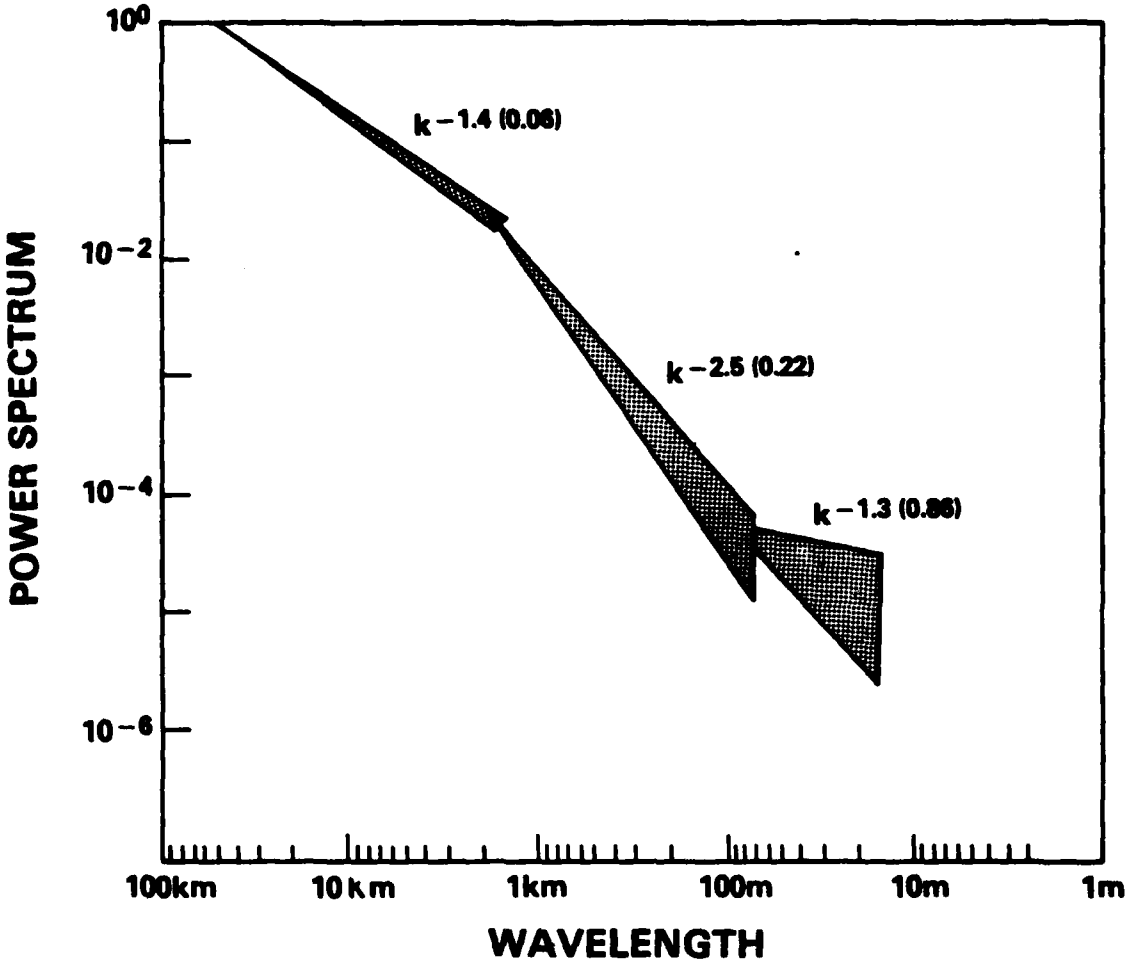

Fig. 10 — Synthesized horizontal power spectral distributions covering the medium, intermediate and transitional wavelength domains.

satellite investigation, providing vertical and horizontal perspectives on the irregularity distributions.

The idea of a hierarchy of instability processes is not new, having been originally suggested by Haerendal (1974). The earliest thoughts pointed to at least two mechanisms with different spectral distributions to account for the discrepancy between the short wavelength extrapolations of $k^{-2.0}$ "in situ" results in the medium-to-intermediate domain and the observed power levels measured by Jicamarca radar at a 3 meter irregularity wavelength. Accumulated information now support 4-5 separate processes and associated spectral distributions covering the medium (λ 2 → 200 km), intermediate (λ 0.2 → 2 km), transitional (λ 20 → 200 m) and short (λ 20 m) wavelength domains. The overall irregularity distribution process can by synoposized as follows:

1) Equatorial spread-F is triggered on the bottomside F-layer gradient by zero-order macrostructures (λ 10's of kilometers) that have evolved from planetary scale waves with sources in solar disturbances and more frequently in meteorological phenomena in the Earth's atmosphere/ionosphere system (e.g., Hines, 1974). A two-fluid process, interacting with background density gradients then results in a turbulent cascade with a $k^{-1.5}$ spectral behavior in the medium-scale irregularity domain (λ 2 → 200 km, see Figures 7 and 10).

2) The existence of medium-scale macrostructure on the bottomside F-layer gradient can then give rise to the Rayleigh-Taylor instability process, filling the intermediate

wavelength domain with a $k^{-2.5}$ spectral distribution. We find the $k^{-2.5}$ intermediate wavelength behavior and the $k^{-1.5}$ medium scale spectral distribution virtually unchanged in their vertical and horizontal projections (See Figures 7 and 10). The km-scale structures which trigger the Rayleigh-Taylor process can also develop from purely random initial conditions (Keskinen, et al. 1982).

3) In the transition wavelength domain ($\lambda \lesssim 200$ m, $kr_i \gtrsim 0.1$) a steeper $k^{-4.7(\pm.3)}$ spectral distribution (e.g. Figure 3) has been determined in specific domains above 282 km populated with gradient-scale lengths $\leq$ 200 m. The altitude limitation should not be interpreted as a direct manifestation of collisional damping since the 282 km regime represents the lowest altitude on the bottomside F-region gradient where 200 m gradient scale lengths have been observed. This lowest region corresponds to the upper boundary of the lowest altitude F-region depletion. While the theoretical work of Gary et al., (1983) points to substantial collisional effects in the lower F-region ($\lesssim$ 250 km), the existing experimental data (this work and that of Kelley et al., 1982a) cannot be interpreted as a confirmation of their predictions.

Our transitional $k^{-4.7(\pm.3)}$ wavelength observations cover the 200-to-20 m domain with the longer wavelength departure from intermediate scale behavior occurring near $kr_i \lesssim 0.1$. Our short wavelength limit on the $k^{-4.7(\pm.3)}$ behavior is at or near $kr_i \approx 1$. As discussed in the text, the spectral behavior is believed to be identified with the universal drift instability driven by

gradient scale lengths $\lesssim$ 200 meters...a conclusion substantiated by the experimentally documented coexistence of $L_n \lesssim$ 200 m and $k^{-4.7(\pm.3)}$ domains.

4) At shorter wavelengths ($\lambda \lesssim$ 20 meter, $kr_i \gtrsim 1$) our results show a marked departure from the longer intermediate-wavelength behavior. The short wavelength results cannot be described by a single (or uniform) spectral distribution but rather by a resonance-like characterization (e.g. Figures 4 and 5). When substantial short wavelength spectral power is observed it is at significantly higher levels than that which would be expected by a $k^{-4.7(\pm.3)}$ intermediate wavelength extrapolation and found to be co-located with the region which provided the most intense high-altitude 1 meter Altair radar returns. Our "in situ" results provide the first documentation of the "softening" of the spectra (e.g. Figure 7) at short wavelengths that was necessary for consistency with ground-based radar observations. Previous experiments lacked appropriate sensitivities.

The intermediate-to-short wavelength breakpoint at $kr_i \lesssim 1$ is consistent with stability criterion for universal drift waves (Huba and Ossakow, 1979); that is, at shorter wavelengths ($\lambda \lesssim 20$ m, $kr_i \gtrsim 1$) the mode experiences ion viscous damping and is less effective. To explain radar results at small wavelengths Huba and Ossakow (1981a) then invoked the kinetic lower-hybrid-drift instability in the $kr_i >> 1$ domain as the most plausible candidate. Their proposal represents an attractive option because the lower-hybrid-drift instability is characterized by strongly magnetized electrons ($\omega << \omega_c^e$, $kr_e \lesssim 1$, $r_e/L << 1$) and

unmagnetized ions ($\omega >> \omega_c^i$, $kr_i >> 1$)...conditions representing a reasonably good fit to our observational domain. Their theoretical results as well as those of Sperling and Goldman (1982) require L < 30 m for instability growth in domains where we have observed intense short wavelength spectra. Analysis of our data showed meaningful lower limits for contributing gradient scale lengths to be in the 50 meter region with very few occurrences at $L \lesssim 30$ m. Regions of our smallest gradient scale lengths are co-located with the observations of strong short wavelength spectral power...and is therefore in qualitative agreement with the suggestion of a lower hybrid-drift wave mode. While the satellite observations of Hoegy et al. (1982) have also supported the lower-hybrid drift wave interpretations, we emphasize that the resonance-like structure in our short wavelength results strongly suggests the possibility of a resonant wave-particle interaction process. This interpretation is particularly attractive because an in-phase resonance of particles and waves permit an energy exchange and wave amplification...precisely that which is required to raise the short wavelength power to levels consistent with ground-based radar observations.

The results presented here as well as those in accompanying references represent a rather intensive investigation of equatorial spread-F irregularities. While all explanations are not as uniquely rigorous as one would like, they represent a very good understanding of active processes controlling the nearly six-decades of equatorial irregularity scale sizes. Further

tests of that understanding has already been undertaken in an attempt to trigger artificial spread-F by chemical injection (Narcisi, et al., 1983). Those results will be forthcoming.

ACKNOWLEDGMENTS

The authors wish to thank Drs. J. Huba and M. Keskinen for their comments and review. In addition, we wish to acknowledge the support of data analysis and P^3 instrument development by the Office of Naval Research under Work Unit A02-11.11 (41-0949), Ionospheric and Stratospheric Interactions, Task Area RR-093-02-44. The Plumex rocket campaign was supported by the Defense Nuclear Agency under Subtask Code 125AAXHX640 and S3-4 operations were supported by the Air Force Space Test Program.

REFERENCES

Basu, S., Basu, S., J. Aarons, J. P. McClure and M. D. Cousins, On the coexistence of kilometer-and meter-scale irregularities in the nighttime equatorial F-region, J. Geophys. Res. 83, 4219, 1978.

Dungey, J. W., Convective diffusion in the equatorial F-region, J. Atmos. Terr. Phys. 9, 304, 1956.

Dyson, P. L., J. P. McClure, and W. B. Hanson, In situ measurements of the spectral characteristics of F-region ionospheric irregularities, J. Geophys. Res., 79, 1497, 1974.

Gary, S. P., P. A. Bernhardt and T. E. Cole, Density drift instabilities and weak collisions, J. Geophys. Res. 88, , 1983.

Haerendel, G., Theory of equatorial spread-F, Report, Max-Planck Inst. fur Phys. and Astrophys., Garching, West Germany, 1974.

Hines, C. O., The ionosphere, in The Upper Atmosphere in Motion, Geophysical Union, Heffernan Press (Worcester, Mass.), Ch. 4, 1974.

Hoegy, W. R., S. A. Curtis, L. H. Brace, N. C. Maynard and R. A. Heelis, Dynamics Explorer observations of equatorial spread-F: Evidence for drift waves, Geophys. Res. L. 9, 993, 1982.

Holmes, J. C. and E. P. Szuszczewicz, A versatile plasma probe, Rev. Sci. Instr. 46, 592, 1975.

Holmes, J. C. and E. P. Szuszczewicz, A plasma probe system with automatic sweep adjustment, Rev. Sci. Instr. 52, 377, 1981.

Huba, J. D. and S. L. Ossakow, On the generation of 3-m irregularities during equatorial spread F by low-frequency drift waves, J. Geophys. Res. 84, 6697, 1979.

Huba, J. D. and S. L. Ossakow, On 11-cm irregularities during equatorial spread-F, J. Geophys. Res., 86, 829, 1981a.

Huba, J. D. and S. L. Ossakow, Diffusion of small scale irregularities duing equatorial spread F, J. Geophys. Res. 86, 9107, 1981b.

Kelley, M. C., G. Haerendel, H. Kappler, A. Valenzuela, B. B. Balsley, D. A. Carter, W. L. Ecklund, C. W. Carlson, B. Hausler, and R. Torbert, Evidence for a Rayleigh-Taylor type instability and unwelling of depleted density regions during equatorial spread F, Geophys. Res. Lett., 3, 448, 1976.

Kelley, M. C. and E. Ott, Two-dimensional turbulence in equatorial spread-F, J. Geophys. Res., 83, 4369, 1978.

Kelley, M. C., R. Pfaff, K. D. Baker, J. C. Ulwick, R. Livingston, C. Rino, and R. Tsunoda, Simultaneous rocket probe and radar measurements of equatorial spread-F transitional and short wavelength results, J. Geophys. Res., 87, 1575, 1982a.

Kelley, M. C., R. C. Livingston, C. L. Rino and R. T. Tsunoda, The vertical wave number spectrum of topside equatorial spread-F: Estimates of backscatter levels and implications for unified theory, J. Geophys. Res. 87, 5217, 1982b.

Keskinen, M. J., E. P. Szuszczewicz, S. L. Ossakow and J. C. Holmes, Nonlinear theory and experimental obvservations of the local collisional Rayleigh-Taylor instability in a descending equatorial spread-F ionosphere, J. Geophys. Res. 86, 5785, 1981.

Livingston, R. C., C. L. Rino, J. P. McClure and W. B. Hanson, Spectral characteristics of medium-scale equatorial F-region irregularities, J. Geophys. Res. 86, 2421, 1981.

Matsushita, S., B. B. Balsley and H. Risbeth, editors, J. Atm. Terr. Phys., Special Issue: Equatorial Aeronomy-I, 43, 516 (1981a).

Matsushita, S., B. B.Balsley and H. Risbeth, editors, J. Atm. Terr. Phys., Special Issue: Equatorial Aeronomy-II, 43, 8 (1981b).

McClure, J. P., W. B. Hanson and J. H. Hoffman, Plasma bubbles and irregularities in the equatorial ionosphere, J. Geophys. Res. 82, 2650, 1977.

Morse, F. A., B. C. Ecker, H. C. Koons, C. J. Rice, W. J. Heikkila, J. H. Hoffman, B. A. Tinsley, J. C. Winningham, A. B. Christensen, R. F. Woodman and J. Pomalaza, Equion, and equatorial ionospheric irregularity experiment, J. Geophys. Res., 82, 578, 1977.

Narcisi, R. S., J. Friel, E. J. Weber, C. Howard, J. Winterbottom, E. P. Szuszczewicz, A. B. Melo, L. E. S. Pinto and S. O. Azambuja, Project BIME compiled participant submissions and general information, Air Force Geophysics Laboratory, Hanscom AFB, MA 01731, 20 August 1983.

Rino, C. L., R. T. Tsunoda, J. Petericks, and R. C. Livingston, Simultaneous rocket-borne beacon and in situ measurements of equatorial spread-F intermediate wavelength results, J. Geophys. Res., 86, 2411, 1981.

Singh, M., E. P. Szuszczewicz and J. C. Holmes, The STP/S3-4 satellite experiment: equatorial F-region irregularities, in Effects of the Ionosphere on Radio wave Systems, (J. M. Goodman, editor) U.S. Govt. Printing Office, p. 228, 1982.

Sperling, J. L. and S. R. Goldman, Electron collisional effects on lower hybrid drift instabilities in the ionosphere, J. Geophys. Res. 85, 3494, 1980.

Szuszczewicz, E. P., Ionospheric holes and equatorial spread-F: Chemistry and transport, J. Geophys. Res. 83, 2665, 1978.

Szuszczewicz, E. P., A. T. Tsunoda, R. Narcisi and J. C. Holmes, Coincident radar and rocket observations of equatorial spread-F, Geophys. Res. Lett., 7, 537, 1980.

Szuszczewicz, E. P. and J. C. Holmes, Equatorial spread-F: "in situ" measurements of electron density, temperature and density fluctuation power spectra, NRL Memorandum Report #4289 (August 25, 1980).

Szuszczewicz, E. P., M. Singh and J. C. Holmes, Satellite and rocket observations of equatorial spread-F irregularities: a two-dimensional model, J. Atm. Terr. Phys. 43, 779, 1981.

Szuszczewicz, E. P., J. C. Holmes and M. Singh, The S3-4 ionospheric irregularities satellite experiment: Probe detection of multi-ion component plasmas and associated effects on instability processes, Astrophys. and Space Sci. 86, 235, 1982a.

Szuszczewicz, E. P., J. C. Holmes, D. N. Walker, M. Singh, P. Rodriguez, M. Swinney and L. Kegley, An atlas of ionospheric F-region structures as determined by the NRL-747/S3-4 ionospheric irregularities satellite investigation, NRL Memorandum Report #4862, July 7, 1982b.

Towle, D. M., VHF and UHF radar observations of equatorial F-region ionospheric irregularities and background densities, Radio Sci., 15, 71, 1980.

Tsunoda, R. T., M. J. Baron, J. Owen and D. M. Towle, Altair: An incoherent scatter radar for equatorial spread-F studies, Radio Sci., 14, 1111, 1979.

Tsunoda, R. T., Backscatter measurements of 11-cm equatorial spread-F irregularities, Geophys. Res. Lett. 7, 848, 1980.

Woodman, R. F. and C. LaHoz, Radar observations of F-region equatorial irregularites, J. Geophys. Res. 81, 5447, 1976.

Woodman, R. F. and S. Basu, Comparison between "in situ" spectral measurements of equatorial F-region irregularities and backscatter observations at 3 m wavelength, Geophys. Res. Lett. 5, 869, 1978.